



OPEN Treatment with fibroblast growth factor 19 increases skeletal muscle fiber size, ameliorates metabolic perturbations and hepatic inflammation in 5/6 nephrectomized mice

Berengère Benoit¹, Alice Beau¹, Émilie Bres^{1,2}, Stéphanie Chanon¹, Claudie Pinteur¹, Aurélie Vieille-Marchiset¹, Audrey Jalabert¹, Hao Zhang³, Priyanka Garg³, Maura Strigini³, Laurence Vico³, Jérôme Ruzzin⁴, Hubert Vidal¹ & Laetitia Koppe^{1,2}✉

Chronic kidney disease (CKD) is associated with osteosarcopenia, and because a physical decline in patients correlates with an increased risk of morbidity, an improvement of the musculoskeletal system is expected to improve morbi-mortality. We recently uncovered that the intestinal hormone Fibroblast Growth Factor 19 (FGF19) is able to promote skeletal muscle mass and strength in rodent models, in addition to its capacity to improve glucose homeostasis. Here, we tested the effects of a treatment with recombinant human FGF19 in a CKD mouse model, which associates sarcopenia and metabolic disorders. In 5/6 nephrectomized (5/6Nx) mice, subcutaneous FGF19 injection (0.1 mg/kg) during 18 days increased skeletal muscle fiber size independently of food intake and weight gain, associated with decreased gene expression of myostatin. Furthermore, FGF19 treatment attenuated glucose intolerance and reduced hepatic expression of gluconeogenic genes in uremic mice. Importantly, the treatment also decreased gene expression of liver inflammatory markers in CKD mice. Therefore, our results suggest that FGF19 may represent a novel interesting therapeutic strategy for a global improvement of sarcopenia and metabolic complications in CKD.

Chronic kidney disease (CKD) is a worldwide public health problem. CKD is widely considered as both a bone and muscle-weakening disease, eventually leading to frailty phenotype, with detrimental effects on overall morbidity^{1–3}. Currently, there is no strategy for combating osteosarcopenia in CKD patients except physical activity which is strongly limited by compliance⁴.

We recently demonstrated that mice treated with human recombinant fibroblast growth factor-19 (FGF19) have larger skeletal muscles and increased muscle fiber surfaces⁵. Likewise, FGF19 increases the size of human myotubes *in vitro*⁵. At a signaling level, FGF19 binds to FGF receptors (FGFR)/ β -klotho complex and induces its hypertrophic effect by activating an extracellular-signal-regulated protein kinase 1/2 (ERK1/2)/ mammalian target of rapamycin (mTOR) pathway⁵. Importantly, FGF19 treatment during one or 2 weeks improves muscle wasting and muscle strength in different experimental models including sarcopenic aged mice and glucocorticoid-treated mice⁵. We further reported beneficial effect of one-week FGF19 treatment on muscle strength and locomotion parameters in a rat model of cerebral palsy⁶. Supporting these data, mice with specific intestinal Fgf15 knockout showed reduced muscle fiber size and altered bone metabolism⁷. Human FGF19, and its mouse ortholog Fgf15, are post-prandial hormones produced by enterocytes from the ileum in the small intestine^{8–10}. FGF15/19 is a master regulator of bile acid metabolism and an important player in lipid and carbohydrate

¹CarMeN Laboratory, INSERM, INRAE, Claude Bernard Lyon 1 University, Pierre Bénite, France. ²Department of Nephrology and Nutrition, Hospices Civils de Lyon, Centre Hospitalier Lyon-Sud, Chemin du Grand Revoyet, 69495 Pierre Bénite, France. ³INSERM U1059, Sainbiose, Jean Monnet University, Saint-Etienne, France. ⁴Department of Molecular Medicine, Institute of Basic Medical Sciences, Faculty of Medicine, University of Oslo, Oslo, Norway. ✉email: laetitia.koppe@chu-lyon.fr

metabolism^{8,9}. Rodent studies showed that the elevation of circulating FGF15/19 levels by pharmaceutical treatment or by transgenic overexpression leads to improved metabolic parameters^{8,11–14}.

FGF19, together with FGF21 and FGF23, belongs to the atypical endocrine family of FGFs⁸. In contrast to the canonical FGFs, endocrine FGFs act as circulating hormones and require either α - or β -klotho as co-receptors to activate their cognate FGFRs. While the metabolic roles of FGF23 and FGF21 have been explored in CKD, the function of FGF19 in the uremic context remains unclear¹⁵. A reduction of FGF19 secretion after a meal test was observed in CKD patients¹⁶, whereas another study reported a positive correlation between FGF19 and glucose parameters in CKD patients¹⁷.

Based on all these data, we hypothesized that FGF19 could be a potential new pharmacological target to counteract the loss of muscle, and to improve glucose homeostasis in CKD. Therefore, the aim of this study was to examine the potential benefits of human recombinant FGF19 treatment on musculoskeletal parameters and glucose metabolism in a mouse model of CKD which associates muscle wasting, renal osteodystrophy and perturbation of glucose homeostasis^{18–21}.

Results

FGF19 protects against muscle wasting in CKD mice. Six weeks after the 2nd surgery, Sham and CKD mice were treated during 18 days with FGF19 or its vehicle (Fig. 1A). In CKD + FGF19 mice, the mean plasmatic concentrations of FGF19 was 508 pg/mL. This corresponds to about twice the average concentrations found in CKD patients (Supplementary Figure 1)^{15,18–20}. At sacrifice, circulating urea levels in CKD mice were significantly increased ($p < 0.001$), reaching values similar to those observed in moderate uremic patients (Fig. 1B)²². The 24 h proteinuria was also increased in CKD mice compared to Sham mice ($p < 0.01$) (Fig. 1C). These altered renal functions were not modified by FGF19 treatment (Fig. 1B, C). Daily food intake assessed between week 2 and 10 was similar in all groups (Fig. 1D). The body weight of Sham, CKD and CKD + FGF19 mice were similar before the two surgeries (Fig. 1E), whereas six weeks after the second nephrectomy, the body weights of CKD mice were significantly lower compared to Sham mice ($p < 0.05$) (Fig. 1E). In all three groups, mice gained similar body weight after the 2nd surgery (Fig. 1F). Compared with Sham mice, CKD mice displayed a significant decrease of epididymal adipose tissue ($p < 0.01$), and FGF19 treatment did not have any impact on uremic lipodystrophy (Fig. 1G).

Before investigating the impact of FGF19 on skeletal muscle of CKD mice, we verified the impact of uremia and FGF19 treatment on the FGF15/19 signaling machinery in soleus muscle. No differences were found regarding the gene expression of the receptor *Fgfr4* and the co-receptor *Klb* (the mouse gene encoding β -Klotho) between the groups (Supplementary Figure 2). Then, because we previously demonstrated that FGF19 prevents muscle wasting by enlarging muscle fiber size and by protecting muscles from atrophy⁵, muscle mass and muscle cross section areas were analyzed in different skeletal muscles. There was no difference regarding tibialis anterior, soleus and gastrocnemius weight among groups (Fig. 1H–J). Histological analysis of tibialis anterior and soleus muscles revealed that although most muscle fibers showed normal morphology with regular and polygonal muscle fibers in Sham mice, the aspect of muscle fibers in CKD mice seemed more irregular (Fig. 2A). Examination of muscle-fiber size distribution in tibialis anterior further revealed that CKD mice had a shift toward small myofibers, as compared to Sham mice (Fig. 2B), resulting in a decrease of mean muscle tibialis anterior fiber area in uremic mice (1083 ± 33.58 vs $1235 \pm 44.2 \mu\text{m}^2$ in Sham mice, $p < 0.05$) (Fig. 2C). As we previously observed in different models of muscle atrophy⁵, administration of FGF19 in CKD mice partially counteracted the decrease of muscle fiber surface induced by CKD (Fig. 2B). FGF19-treated CKD mice clearly presented a substantial rightward shift in the distribution of myofiber sizes (Fig. 2B, E–F), with a trend of increased cross-sectional area average in tibialis anterior myofibers (1206 ± 57.91 vs $1083 \pm 33.58 \mu\text{m}^2$ in CKD mice, $p = 0.07$) (Fig. 2C). Similarly, in the soleus muscle, the treatment with FGF19 also counteracted the CKD-induced defects in muscle fiber size, with a reduction of the number of small myofibers and an increase of myofibers within the range 1200 – $2200 \mu\text{m}^2$ (Fig. 2G–K). These results clearly showed that hypertrophic effect of FGF19 treatment is observed in two types of muscles (glycolytic tibialis anterior and oxidative soleus). In soleus, CKD mice were characterized by a higher expression of fast myosin genes (*Myh4* ($p < 0.05$) and *Myh1* ($p = 0.11$)) when compared to Sham animals, and FGF19 treatment tended to reduce this overexpression. However, when the fiber type was assessed by a myosin ATPase staining, we found that the proportion of type I and IIA/B fibers were not different between the groups (Supplementary Figure 1).

As skeletal muscle atrophy in CKD can result from several interrelated mechanisms leading to an imbalance between protein synthesis and degradation^{4,23}, we further investigated whether the beneficial effects of FGF19 could implicate pathways such as the ubiquitin–proteasome or myostatin. Atrophy-related ubiquitin ligases *Atrogin-1* (+29%, $p < 0.01$), and *Murf1* (+14%, $p = 0.06$) were upregulated in soleus muscles from CKD mice as well as *Myostatin* (+132%, $p < 0.01$) (Fig. 3A–C). Treatment with FGF19 decreased significantly the expression of *Myostatin* ($p < 0.05$) (Fig. 3A) and reduced, albeit not significantly, *Murf1* ($p = 0.17$) (Fig. 3C). The treatment had no impact on *Atrogin-1* expression (Fig. 3B). Because it was proposed that the cytokine interleukin-6 (IL-6) in skeletal muscles contributes to energy metabolism and to the regulation of muscle mass²⁴, we also measured the changes in *Il-6* mRNA abundance in muscles. There was no difference in *Il-6* expression in soleus muscle between Sham and CKD mice, but FGF19 treatment significantly increased *Il-6* mRNA levels (Fig. 3D). The gene expression of other inflammatory markers in soleus, like *Mcp1*, was not different between the groups (Fig. 3E). Given that reactive oxygen species (ROS) can play an important role in skeletal muscle atrophy and that some data suggest that FGF19 can attenuate oxidative stress¹², we also measured the expression of key enzymes of oxidative stress defense in soleus. Results did not reveal any differences between groups (Supplementary Figure 4).

Bone loss is often correlated with muscle wasting in CKD^{20,25,26}. We postulated that FGF19 treatment could eventually improve bone quality in parallel to its beneficial action on muscle parameters. As expected, the

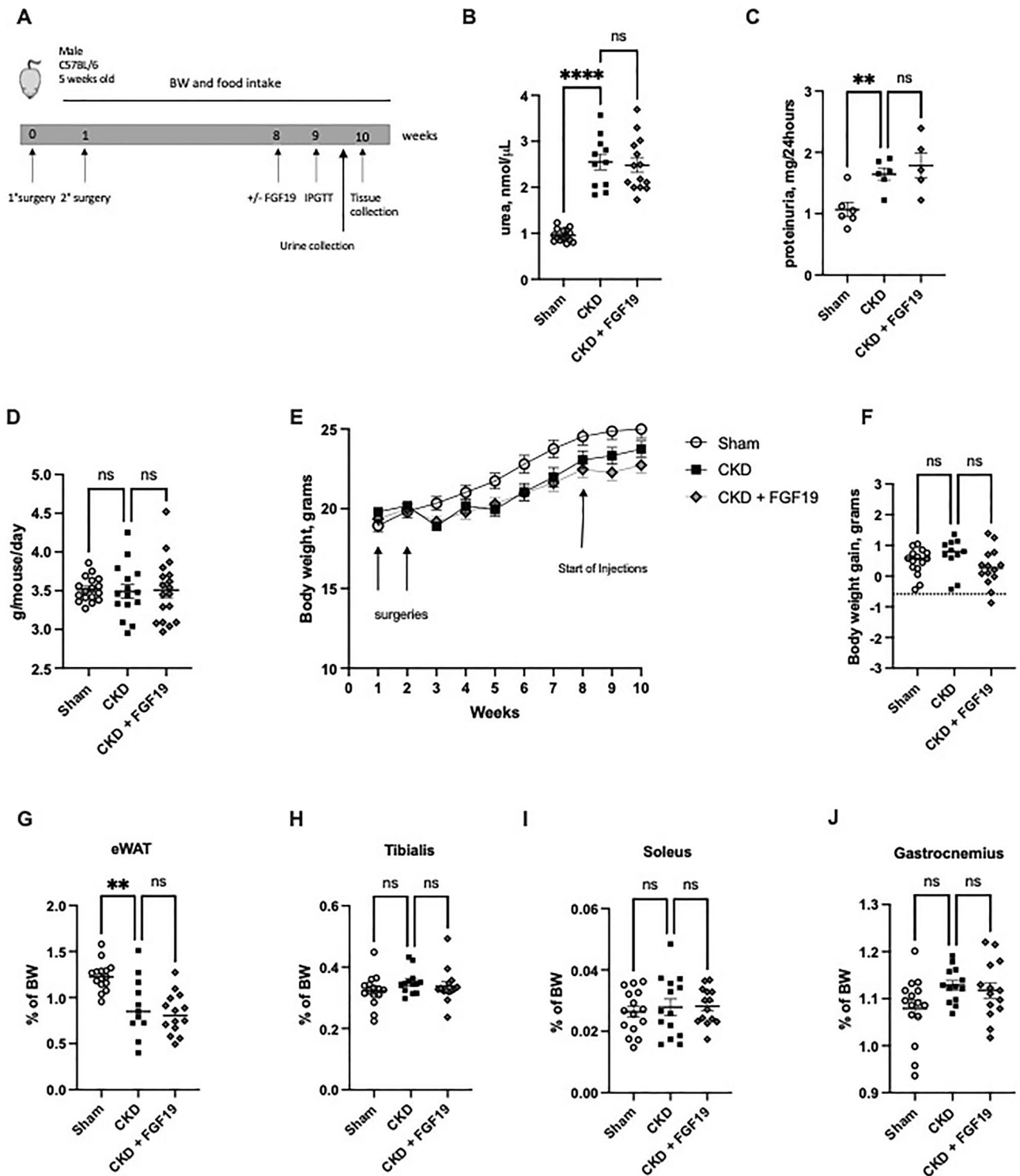


Figure 1. FGF19 treatment does not modify food intake and body composition in uremic mice. CKD mice induced by 5/6 nephrectomy or Sham mice were treated with 0.1 mg/kg body weight of FGF19 or with vehicle during 18 days. (A) Experimental timeline. (B) Blood urea. (C) 24 h proteinuria. (D) Daily food intake. (E) Body-weight evolution. (F) Body-weight gain. (G) Weight of epididymal WAT. (H) Weight of tibialis anterior, and (I) Weight of soleus (J) Weight of gastrocnemius after FGF19 or vehicle injection. n = 13–15 mice per group expected for proteinuria (n = 5–6). Data are mean ± SEM. Statistical analysis was done using a one-way ANOVA test. *P < 0.05, **P < 0.01, ****P < 0.0001. Abbreviation: BW: body weight, CKD: chronic kidney disease., n.s., not significant; WAT: white adipose tissue.

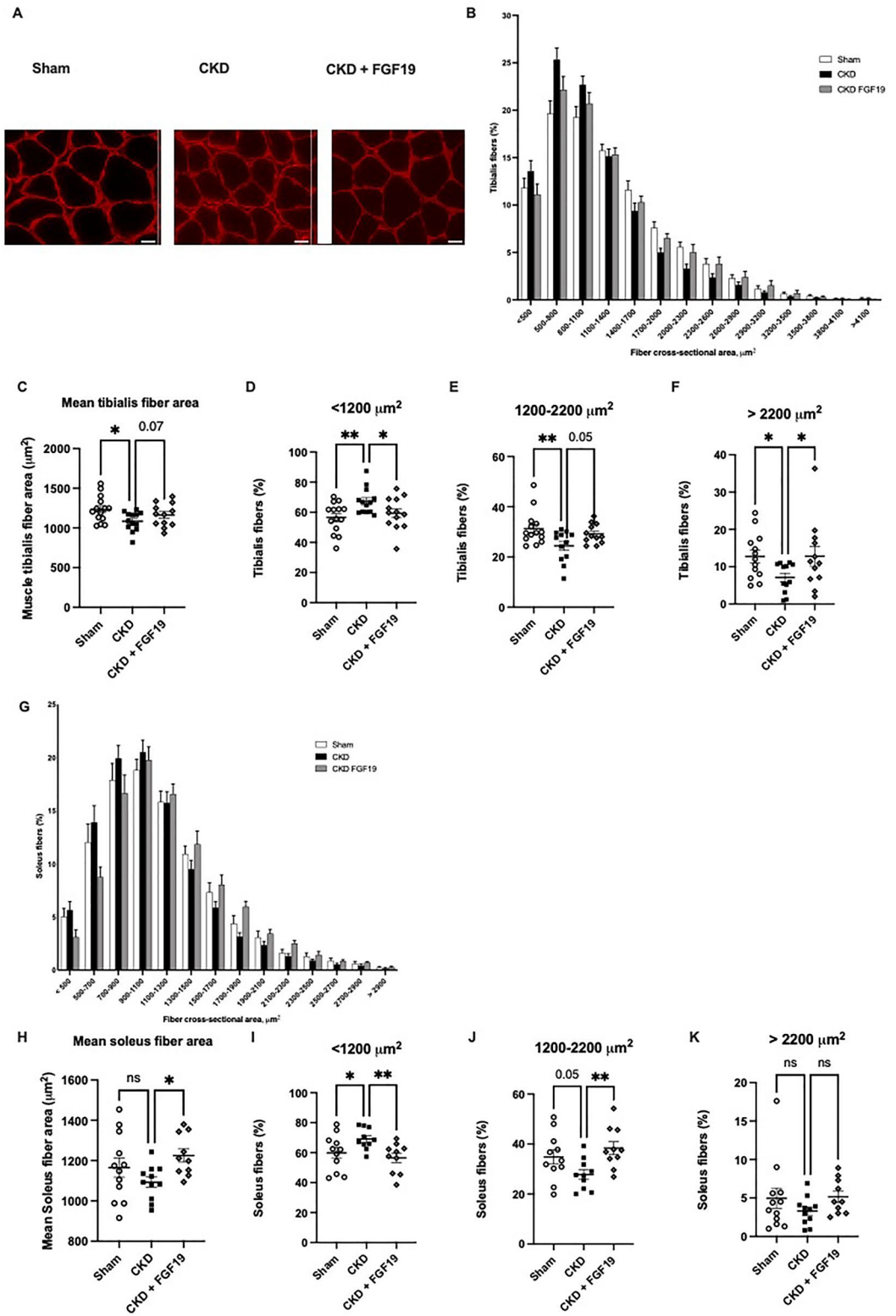


Figure 2. FGF19 treatment induces skeletal muscle hypertrophy in CKD mice. (A) Pictures are representative images of laminin-stained tibialis anterior muscles (n = 6–12 images per mouse), scale bar = 50 μm . (B) Frequency distribution of cross-sectional tibialis anterior fiber area. (C) Mean tibialis anterior fiber area. Distribution of fibers in tibialis anterior (D) $<1200 \mu\text{m}^2$, (E) between 1200 and 2200 μm^2 and (F) $>2200 \mu\text{m}^2$. (G) Frequency distribution of cross-sectional soleus fiber area. (H) Mean soleus fiber area. Distribution of fiber in soleus (I) $<1200 \mu\text{m}^2$, (J) between 1200 and 2200 μm^2 and (K) $>2200 \mu\text{m}^2$. Data are mean \pm SEM. n = 11–15 mice per group. Statistical analysis was done using a one-way ANOVA test. * $P < 0.05$, ** $P < 0.01$. Abbreviation: CKD: chronic kidney disease, n.s., not significant.

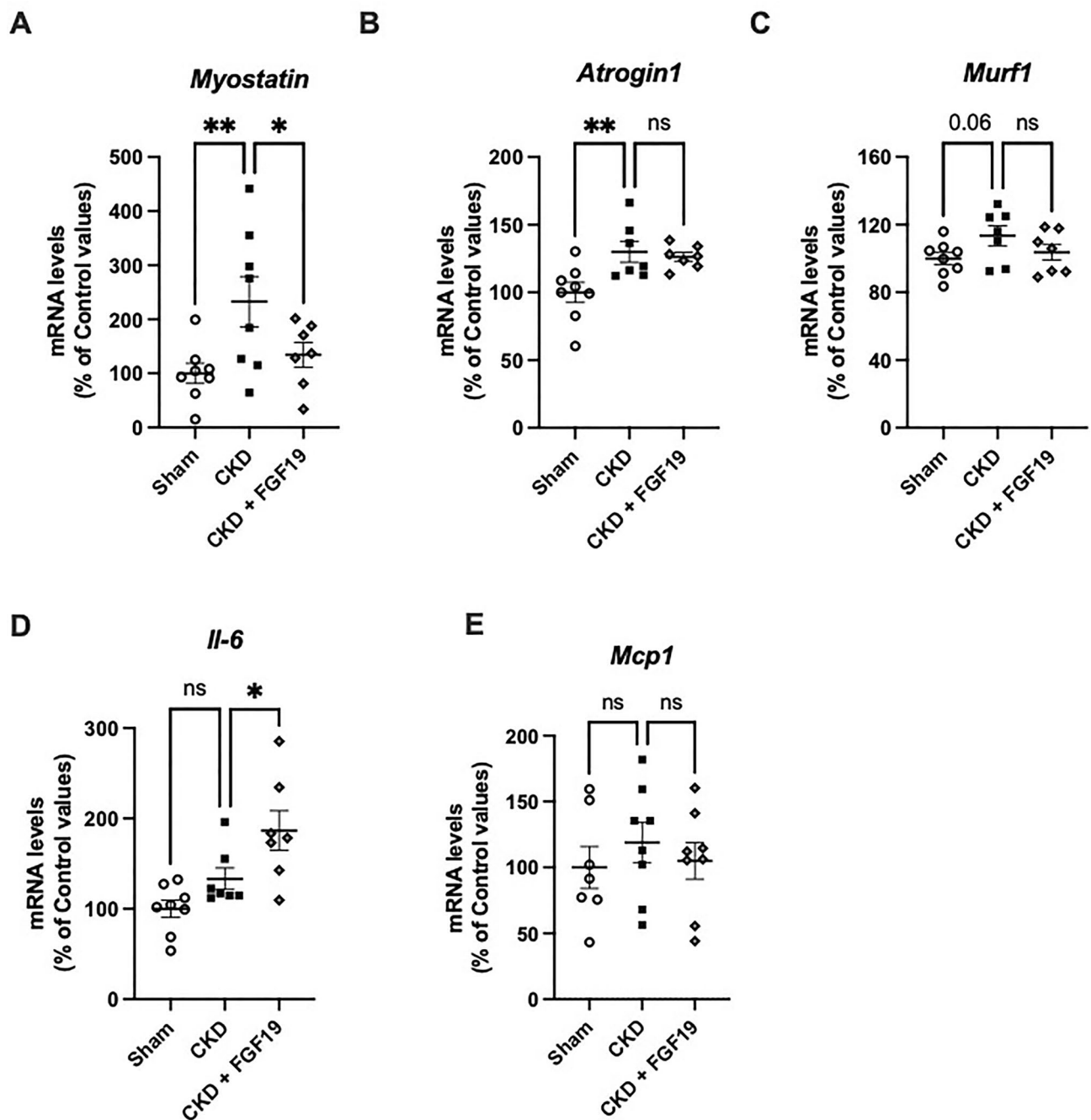


Figure 3. FGF19 partially decreases expression of negative regulators of muscle mass in soleus of CKD mice. Relative mRNA expression of (A) *Myostatin* (B) *Atrogin1* (C) *Murf1* (D) *Il-6* and (E) *Mcp1* in Sham and CKD mice after FGF19 or vehicle treatment. *Tbp* (TATA-Box Binding Protein) was used as reference gene to normalize the results. Results are expressed as the ratio of target mRNA levels to housekeeping gene mRNA levels and normalized to the levels in Sham mice. Data are expressed as mean \pm SEM for $n=7-8$ animals in each group. Statistical analysis was done using a one-way ANOVA test $*p < 0.05$, $**p < 0.01$. Abbreviation: CKD: chronic kidney disease., *Il-6*: interleukin-6, *Mcp1*: monocyte chemoattractant protein 1, n.s., not significant.

experimental CKD model induced a loss of bone, independently of body weight and diet (Supplementary Figure 5). CKD was associated with an increase in cortical porosity, a decrease in cortical thickness and a lower mineralization (tissue mineral density) without modification of the trabecular structure (Supplementary Figure 5B–H). However, the 18-days FGF19 treatment was not associated with any detectable effect on these bone structural parameters (Supplementary Figure 5A–H).

FGF19 improves whole-body glucose tolerance and reduces hepatic expression of gluconeogenesis-related genes. CKD mice had higher fasting plasma glucose levels (170.7 ± 3.3 mg/dl in CKD

mice vs 151.3 ± 7.7 mg/dl in Sham mice, $p < 0.01$) (Fig. 4A), and were glucose intolerant, as assessed by ip-GTT (Fig. 4B). After treatment with FGF19, the CKD mice displayed a marked reduction in their glucose excursion during ip-GTT (area under curve (AUC) $12,573 \pm 456$ vs. $16,693 \pm 2465$ mg/dl min⁻¹, $p < 0.0001$, in FGF19-treated CKD mice vs CKD mice) (Fig. 4B, C).

The metabolic effects of FGF19 in the liver have been previously linked to a stimulation of hepatic glycogen metabolism and a reduction of gluconeogenesis through an insulin-independent pathway⁹. We found that treatment with FGF19 increased the hepatic gene expression of the regulatory subunit p85 of the *Pi3k* gene (Fig. 4D) and of glycogen synthase 2 (*Gys2*) (Fig. 4E) and reduced the expression of glucose-6-phosphatase (*G6pc1*) (Fig. 4F).

In addition to changes in liver metabolism, we previously reported that ectopic lipid accumulation in muscle correlates with insulin resistance in CKD mice model²⁷. Here we found using an Oil Red O staining that lipid droplet infiltration was increased in soleus muscle of CKD mice and that FGF19 treatment mitigated this accumulation of lipids (Fig. 4G and J). Furthermore, in agreement with previous findings²⁷, the ectopic accumulation of fat in skeletal muscle was correlated with insulin resistance parameters (Fig. 4H, I).

FGF19 attenuates hepatic inflammation in CKD mice. Previous works have demonstrated a chronic state of inflammation in CKD models. Here, we found that CKD was associated with elevated expression of several inflammatory markers in the liver. Liver of CKD mice had increased gene expression of inflammatory cytokines (e.g. *Il-1 β* , *Il-6*, *Tnfa*), of *Mcp1*, a chemokine that recruits and activates macrophage, of *Foxo1* a master regulator of inflammation and of *Myd88* a central adaptor of innate immunity. Interestingly, FGF19 treatment reduced significantly the expression levels of all these inflammatory markers (*Foxo1*, *Myd88*, *Mcp1*, *Il-6*, *Tnfa*, and *Il-1 β*) in the livers of CKD mice (Fig. 5A–F). However, the levels of TNF α and IL-6 proteins measured by ELISA in liver extracts were very low and were not different between the groups (Supplementary Figure 6).

Discussion

Muscle wasting is a well-established complication of CKD, which significantly worsens the quality of life of CKD patients^{1–3}. This muscle deterioration is poorly understood, but likely involves multiple biological mechanisms⁴. Yet, no readily available treatment for successfully preventing muscle wasting in CKD exists. In this study, we tested the potential of FGF19 to protect skeletal muscle in 5/6 nephrectomized mice as a CKD model. Our results demonstrated for the first time that subcutaneous injections of human recombinant FGF19 during 18 days in uremic mice is able (1) to improve fiber size of skeletal muscles (2) reverse glucose intolerance and (3) improve the gene expression of inflammatory markers in the liver.

We have confirmed that FGF19 can be a promising agent to treat muscle wasting through increasing skeletal muscle fiber size^{5,6}. In previous studies, we demonstrated that treatment with FGF19 during one or 2 weeks improved muscle wasting and muscle strength in different experimental models including sarcopenic aged mice and glucocorticoid-treated mice, but also found that FGF19 could have an anabolic effect in normal mice and in human myotubes⁵. In the present experiments, we further strengthened the therapeutic potential of FGF19 by demonstrating its ability to counteract CKD-induced muscle atrophy. In our previous works⁵, we demonstrated that the hypertrophic effects of FGF19 on skeletal muscle fibers is mediated by the ERK/mTOR signaling pathway. Although we did not directly examine this pathway in the present work, we are expecting the same mechanism because the effect of FGF19 on muscle fiber size, without affecting fiber type composition, is rather similar to the one observed previously. However, one cannot exclude that other pathways might be also involved due to the uremic condition. This remains to be investigated specifically in further studies.

This beneficial effect of FGF19 treatment on muscle fiber surface was associated with the suppression of myostatin expression and interestingly with an overexpression of *Il-6* in soleus muscle. IL-6 is a pleiotropic cytokine, which is produced by muscle fibers as a myokine with critical action on muscle homeostasis, adapting glucose uptake to the energy requirements during exercise or stress²⁸. It is important to note that we did not observe any changes in the gene expression of other inflammatory markers in the soleus muscle of CKD mice with or without FGF19. This suggested therefore that the overexpression of *Il-6* is not reflecting an inflammatory state in the muscle but rather a specific induction of the myokine. This finding suggests therefore a potential role of IL-6 in the effect of FGF19 on skeletal muscle homeostasis, which remains to be further investigated in different physiological conditions.

In the present CKD mouse model, the effect of uremic environment was mainly found on the size of the muscle fibers whereas muscle mass did not appear altered. Also, the repartition of fibers in CKD mice was very modestly modified. This differs from previous observations reporting decreased muscle mass, a decrease of type I and IIA fibers and an increase of type IIB fibers in the majority of CKD rodent models^{19,29,30}. The difference may be due to the diet since we used a standard chow diet (17% proteins) while others^{19,29,30} fed mice with 40% proteins in order to increase uremic intoxication and catabolism. Also, our mice were younger and presented a less advanced CKD than in previous reports^{31,32}. Nevertheless, the important observation here is the effects of FGF19 on muscle fiber surface and on the expression of genes related to muscle atrophy. In addition, it is important to note that FGF19 treatment was started 6 weeks after the second nephrectomy and not immediately after uremic induction, as it was generally done for other treatments, such as leptin receptor antagonist or myostatin inhibitors^{19,33}. This may support FGF19 for curative treatment for uremic myopathy beside to be a preventive strategy.

The role of FGF19 on bone metabolism has remained poorly explored. A recent study suggested that Fgf15 is important to prevent bone loss after bariatric surgery in obese mice⁷. However, in the present CKD model, we failed to detect any effect of FGF19 treatment on bone parameters. The lack of effect of FGF19 while clear

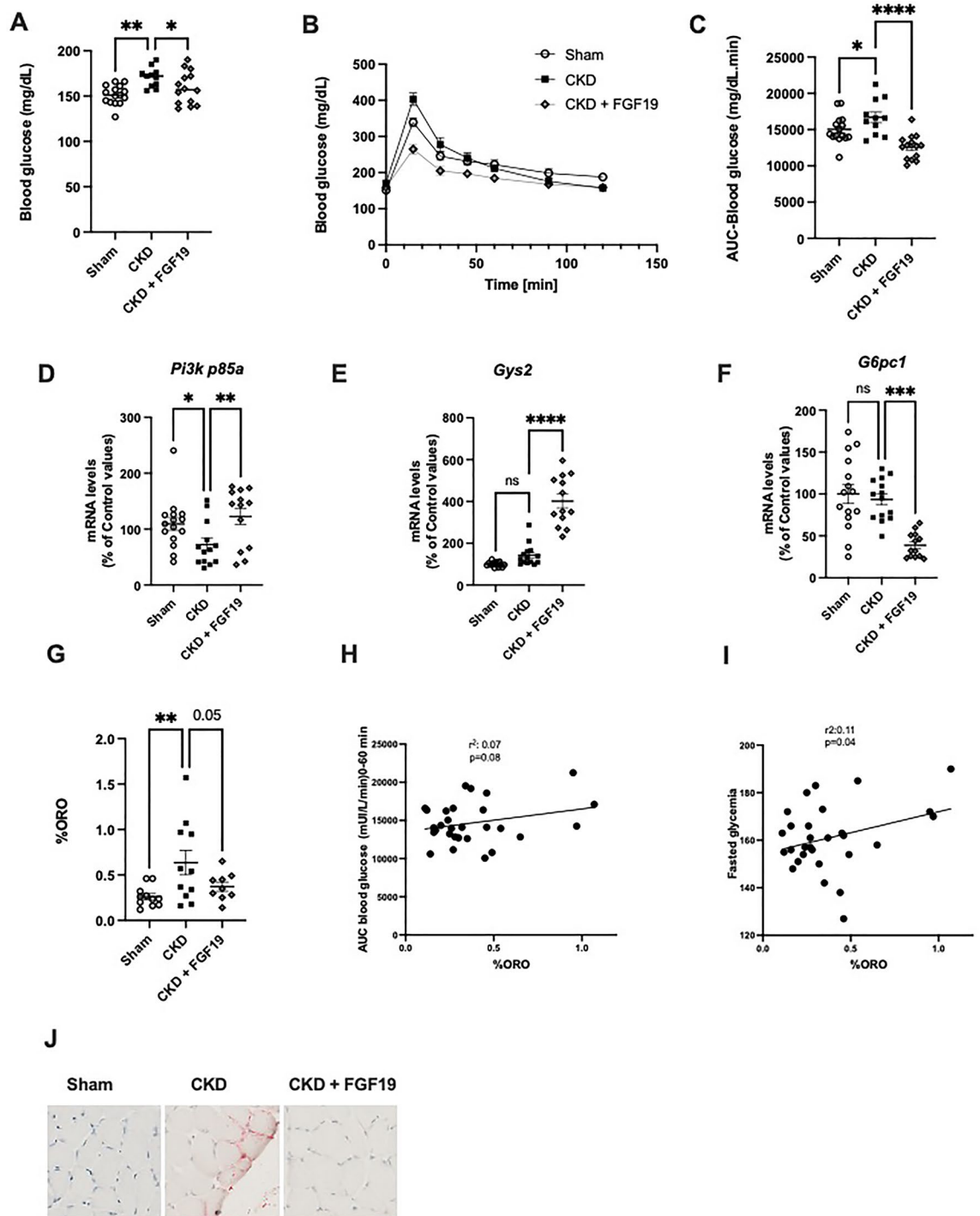


Figure 4. FGF19 corrects uremia-mediated insulin resistance in association with suppressed hepatic gluconeogenesis genes expression. (A) Fasted blood glucose. (B) Glucose levels during an i.p. GTT (2 g/kg) and (C) AUC (0–60 min) in control and CKD mice after FGF19 or vehicle treatment. Relative mRNA expression of (D) *Pi3k p85a* (E) *Gys2* and (F) *G6pc1* in Sham and CKD mice after FGF19 or vehicle treatment. (G) Percentage of Oil Red O staining of soleus muscle in Sham and CKD mice after FGF19 or vehicle treatment. Relationship between Oil Red O staining of soleus muscle and (H) fasted glycemia or (I) AUC glucose during ip-GTT. (J) Representative images of muscle sections stained with Oil Red O. *Tbp* (TATA-Box Binding Protein) was used as reference gene to normalize the results. Results are expressed as the ratio of target mRNA levels to housekeeping gene mRNA levels and normalized to the levels in Sham mice. Data are expressed as mean \pm SEM for $n=9$ – 15 animals in each group. Statistical analysis was done using a one-way ANOVA test * $p < 0.05$, ** $p < 0.01$, *** $p < 0.001$. Abbreviations: AUC: area under curve, CKD: chronic kidney disease, *G6pc1*: glucose-6-phosphatase, *Gys2*: glycogen synthase, *Pi3k*: phosphoinositide 3-kinase, n.s., not significant.

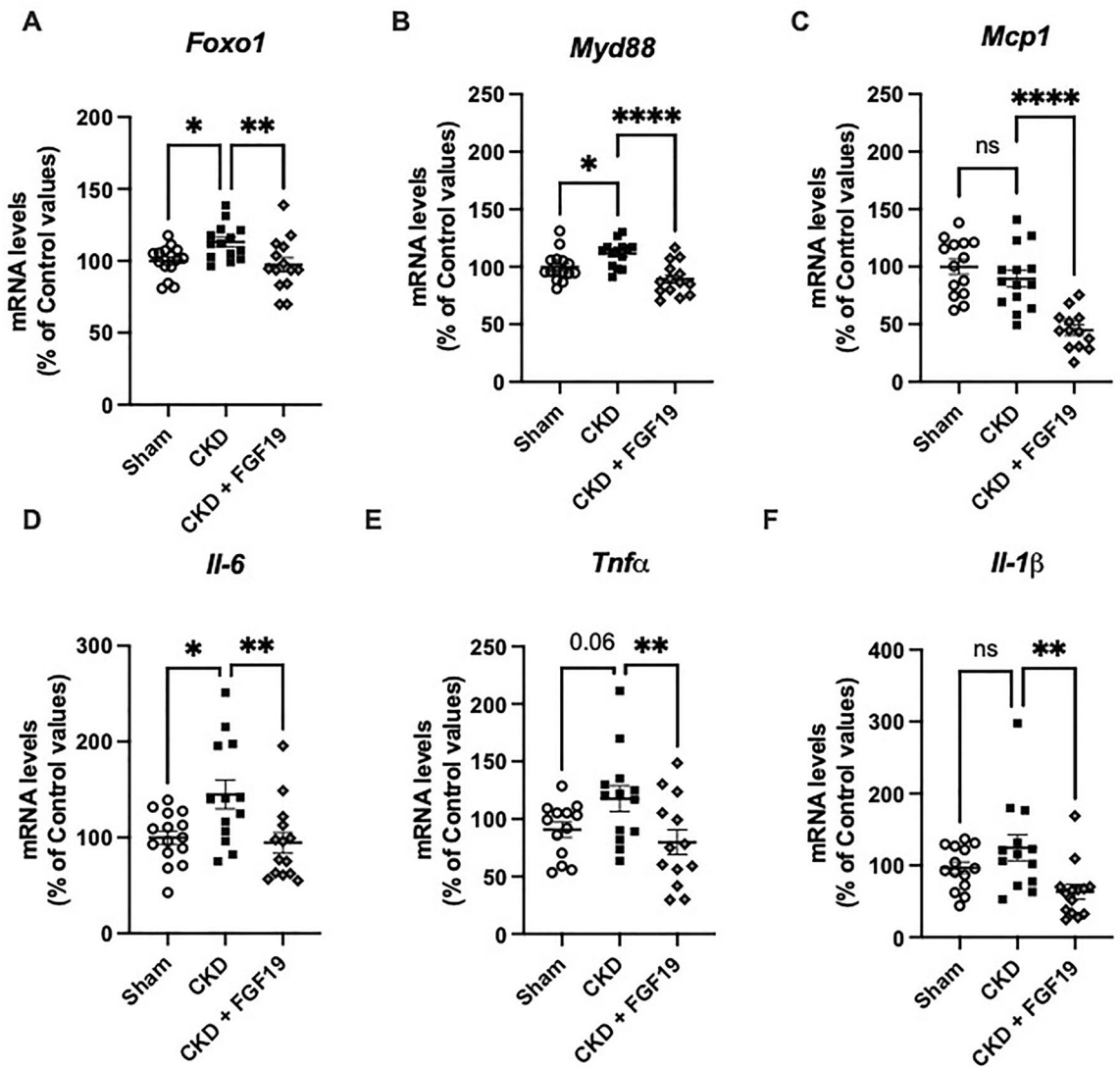


Figure 5. FGF19 reduces hepatic metabolic inflammation in CKD mice. Relative mRNA expression of (A) *Foxo1* (B) *Myd88* (C) *Mcp1* (D) *Il-6* (E) *Tnfa* and (F) *Il-1 β* in Sham and CKD mice after FGF19 or vehicle treatment. *Tbp* (TATA-Box Binding Protein) was used as reference gene to normalize the results. Results are expressed as the ratio of target mRNA levels to housekeeping gene mRNA levels and normalized to the levels in Sham. Data are expressed as mean \pm SEM for $n = 13$ – 15 animals in each group. Statistical analysis was done using a one-way ANOVA test * $p < 0.05$, ** $p < 0.01$, *** $p < 0.001$. Abbreviation: CKD: chronic kidney disease, *Foxo1*: Forkhead box protein O1, *Il*: interleukine *Mcp1*: monocyte chemoattractant protein 1, *Tnfa*: Tumor Necrosis Factor alpha, n.s., not significant.

alterations were seen in the control CKD mice, may suggest that 18 days of treatment were not sufficient to impact bone parameters at a measurable level.

In agreement with previously published data using obese rodent models, we found that FGF19 did ameliorate glucose intolerance induced by CKD. Previous studies reported elevated hepatic glucose production in chronically uremic patients³⁴ and also in CKD mice³⁵. Inhibition of hepatic gluconeogenesis by FGF15/19 was previously observed in rodents^{8,36}, and we found in the liver of CKD mice that FGF19 treatment reduced the expression of *G6pc1*, the rate limiting enzyme of gluconeogenesis. In addition, FGF19 stimulated the hepatic expression of *Gys2*, the main hepatic isoform of glycogen synthase. Together with the higher expression of p85subunit of *Pi3kinase* in the presence of FGF19, these data provided some mechanistic insights supporting the beneficial action of FGF19 on liver glucose metabolism and insulin action. Interestingly, studies have demonstrated that FGF19 levels is negatively correlated with fasting glucose and insulin levels in CKD patients^{16,17}.

Previous data have shown that exogenous administration or genetic overexpression of FGF15 could decrease body weight and adiposity^{11–13} in healthy and pathological conditions. CKD mice have an increase of resting energy expense that participates to the development of sarcopenia³⁷. In our study, we observed that treatment with FGF19 during 18 days did not change the final body weight and weight gain of CKD mice, suggesting that FGF19 does not affect energy expenditure in this model. Further studies are needed to explore more deeply this

difference, which could be related to the conditions of the treatment or eventually to a specificity of the FGF19 action in the uremic context.

Hepatic inflammation is commonly observed in different CKD mice model¹⁹ and is associated with an increase in proinflammatory cytokines. Interestingly, we observed that, after 18 days of treatment with FGF19, the expression of several inflammatory markers in the liver of CKD mice was strongly inhibited. We found no difference in the amount of inflammatory proteins in the liver, but their levels were very low, limiting the possibility to highlight any potential statistical differences. Although the role of FGF19/15 on inflammation remains poorly documented, our findings are consistent with decreased hepatic inflammation and reversed liver injury in response to FGF19 treatment observed in a mouse model of primary sclerosing cholangitis³⁸. Further studies are needed to investigate the potential anti-inflammatory action of FGF19.

All these preclinical data support a promising effect of FGF19 to fight metabolic alterations and skeletal muscle wasting in CKD. The effect of FGF19 itself has possibly CKD-independent effects on muscle and liver as previously published^{5,8,36}. However, one cannot exclude additional actions of FGF19 on specific CKD defects. For example, uremic environment causes a lower density of growth hormone (GH) receptor and post-receptor defects in GH signal transduction, characterized by impaired phosphorylation and nuclear translocation of GH-activated STAT proteins³⁹. This hormonal resistance could explain the failure of the positive effects of recombinant human growth hormone (hGH) in stable hemodialysis patients on lean body mass⁴⁰. As a growth factor acting through an alternative signaling pathway compared to GH, FGF19 could eventually overcome this defect. Similarly, the effect of FGF19 on hepatic inflammation markers has not been evidenced so far¹⁴. We observed that the expression of genes related to inflammation are strongly down-regulated in CKD mice treated with FGF19. Further studies are thus needed to determine if FGF19 beneficial action in CKD mice could be related to different pathways than those previously described in a non-uremic context.

FGF15/19 acts by activating FGFR homodimers complexed with the membrane bound protein β -Klotho. CKD is characterized by a decrease of α -klotho gene and protein expression in kidney, and a lower level of circulating soluble α -klotho⁴¹. Also, CKD is associated with a decrease of *Fgfr4* expression in kidney tissue⁴¹. However, the impact of CKD on the FGFR- β -Klotho pathway in muscles has never been explored. In this study, we did not see any difference on gene expression of *Fgfr4* and *Klb* in muscles of CKD mice and after FGF19 treatment. Several studies have reported an increase of FGF19 plasmatic levels in hemodialyzed patients^{22,42}, suggesting that beyond renal accumulation, the high level of FGF19 in CKD could reflect a resistance of endogenous FGF19. We can state the hypothesis that the potential FGF19-resistance is not primarily due to a lowered *Fgfr4* and *Klb* expression in muscles but potentially by impaired signal transduction. Therefore, our study is important to validate the proof of concept of the efficacy of FGF19 treatment in uremic context and in CKD patients.

In one clinical study, FGF19 secretion after a meal test was decreased in hemodialyzed patients¹⁶. FGF15/19 is produced by the ileal enterocytes and is released into the enterohepatic circulation postprandially in response to bile acids via activation of the farnesoid X receptor (FXR). Gut microbiota, as an indispensable participant in bile acids metabolism, is responsible for conversion of primary bile acids into secondary bile acids in the gut lumen and also for changes in the levels of several bile acid metabolites that could have different ability to activate FXR⁴³. CKD is characterized by an intestinal dysbiosis⁴⁴ and a modification of bile acids composition (decrease in the proportion of primary bile acids and increase in the proportion of secondary bile acids)⁴⁵. Given these observations, it could be hypothesized that perturbations of bile acids metabolism linked to dysbiosis associated with CKD may have contributed to the reduced postprandial FGF19 response in this population¹⁶. Understanding the interplay between intestinal microbiota, bile acids metabolism and FGF19 secretion in CKD needs complementary studies.

This study has several limitations that deserve some comments. Firstly, as mentioned before, the CKD mice did not display a severe skeletal muscle atrophy and bone modifications. Previous studies highlighted an alteration of muscle function already measurable in young (12–15 weeks) 5/6 nephrectomized mice (like our model)^{31,46} despite that muscle volume and power are preserved, but generally, mineral and bone disorders are more intense in CKD mice 1 year after the nephrectomy^{20,31}. Here we used juvenile mice of 6 weeks. It will be interesting to examine the long-term effects of FGF19 on skeletal muscle atrophy and potentially on bone parameters in an ageing-CKD model. Secondly, the study was performed in male mice only. Some studies have observed that the intensity of muscle wasting is less important in female mice in CKD models suggesting that the potential effect of FGF19 may be less significant in this population⁴⁷. Also, Jia et al. reported that the expression of *Fgf15* is higher in the skeletal muscle of female mice than that of male mice. Fasting reduces *Fgf15* expression in female muscles but had no effect on male muscles⁴⁸. The mechanisms underlying these gender differences are currently unknown and gender differences in FGF19 have never been explored and need further studies. Also, another important limitation of the present work is the fact that muscle function and muscle strength have been not measured. However, in all our previous studies, we have clearly demonstrated that the increase of muscle fiber size is associated with an increase of muscle strength^{5,6}. Such association has been also found in CKD mice model^{29,49}. Finally, a limitation for using FGF19 in human is the potential risk of hepatocellular carcinoma, as shown in transgenic mice overexpressing FGF19⁵⁰. It has been observed that FGF19, as a growth factor, can stimulate tumor growth and invasion and promote several cancer types, including breast, prostate and colon cancer⁵¹. Interestingly, engineered FGF19 analogues devoid of pro-carcinogenic activity have been developed^{36,52} and one of them, Aldafermin (also known as NGM282 or M70), is currently in clinical development for the treatment of nonalcoholic steatohepatitis³⁶. Aldafermin efficacy on skeletal muscle and potentially in CKD, remains to be evaluated.

In conclusion the presented preclinical data support a possible translational application of FGF19 therapy, or its analogues, in CKD patients. Without available treatment for CKD-associated sarcopenia validated to date, this novel strategy could provide a new way for the preservation of muscle mass in these patients.

Materials and methods

Animals. We confirm that all experimental protocols were approved by the local ethic committee named “comité d'éthique en expérimentation animale de la Région Rhône-Alpes, Lyon, France” (CECAPP # LS_2019_004). All experimental procedures were performed in accordance with the guidelines laid down by the French Ministry of Agriculture (no 2013–118) and the European Union Council Directive for the protection of animals used for scientific purposes of September 22nd, 2010 (2010/63UE). We confirm that all methods were carried out in accordance with relevant guidelines and regulations. We confirm that all methods are reported in accordance with ARRIVE guidelines (<http://www.nc3rs.org.uk/arrive-guidelines>). We confirm that during the surgery and the euthanasia, we have employed anesthesia consistent with the commonly accepted norms of veterinary best practice. All efforts were made to minimize the number of animals used and their suffering. The required sample size was calculated by a power analysis before the start of the experiment. Male C57BL/6j mice were group-housed in an air-conditioned room with a controlled environment of 21 ± 0.5 °C and 60–70% humidity with a 12 h light/dark cycle. Moderate CKD was induced by 5/6 nephrectomy with a 2-steps surgical procedure in 5-weeks-old male mice as previously described under anesthesia ketamine/xylazine (100 mg/kg and 20 mg/kg, intraperitoneal respectively)¹⁸. Sham mice underwent two mock surgeries. Body weight and food intake were measured once a week. Recombinant human FGF19 (R&D System, UK) was injected subcutaneously every day at 0.1 mg/kg during 18 consecutive days, 6 weeks after the second nephrectomy. The controls were injected with the vehicle solution, which consists of a phosphate buffer solution (PBS) with 0.1% of bovine serum albumin (BSA)). We had three groups of 15 mice: (1) Sham treated with vehicle solution; (2) CKD treated with vehicle solution and (3) CKD treated with FGF19. Two days before the end of the experiment, mice, by two, were placed in metabolic cages in order to collect the urine produced over 24 h. At the end of the study, mice were euthanized with anesthetic ketamine/xylazine (100 mg/kg and 20 mg/kg, intraperitoneal respectively).

Glucose tolerance test, tissues and blood collection. For intraperitoneal glucose tolerance test (ip-GTT), animals were injected i.p. with 2 g of D-glucose/kg of body weight after a 5-h fast. D-glucose was diluted at 20% in PBS before the ip-GTT. Blood glucose was measured prior to and 15, 30, 45, 60, 90, and 120 min after the i.p. injection of D-glucose. Blood glucose values were determined from a drop of blood sampled from the tail using an automatic glucose monitor (Accu-Check® Performa, RocheDiabetes), as previously reported.¹⁸

One week after the ip-GTT, mice were euthanized with ketamine/xylazine (70/4 mg/kg). Plasma was collected and stored at -80 °C. Skeletal muscles, liver and epididymal white adipose tissue were removed, and weighted. Only liver, soleus and tibialis muscles were snap-frozen in liquid nitrogen and then stored at -80 °C until analysis. A sample of soleus and tibialis anterior muscles from the controlateral leg were embedded in OCT-tissue freezing medium (General Data) for histological analysis. The mouse leg, without muscle tissue, was then stored in ethanol 80% at 4 °C until further bone-related analysis.

Plasma urea levels were measured using a commercial colorimetric assay kit (Sigma). Groups of two mice were placed in metabolic cages to collect urine during 24 h. Total protein levels in urine samples were determined using a standard Bradford protein assay (Bio-Rad Laboratories).

Plasma FGF19 concentrations were measured using a commercial colorimetric assay kit (R&D Systems).

Gene expression analysis and inflammatory protein assays. Total RNAs from soleus muscles and livers were extracted using TRI Reagent® (Sigma Aldrich). Purity and concentration of RNA were determined using NanodropOne (Ozyme) and quality checked using Bioanalyser (Agilent). First-strand cDNAs were synthesized from 1 µg of total RNAs using PrimeScript RT kit reagent kit (Perfect Real Time) (Takara Bio Europe). Real-time qPCR assays were performed on 1/20 diluted cDNA using TB Green Premix Ex Taq (Tli RNaseH plus) (Takara Bio Europe) with Rotor-Gene 6000 (Qiagen) using TB Green Premix Ex Taq (Tli RNaseH plus) (Takara Bio Europe) as previously described⁵³. TATA-box binding protein (*tbp*) was used as a reference gene to normalize the results. Results are the ratio of target mRNA levels to *tbp* mRNA levels and are expressed as percentage of the Sham group values. Primers sequences are listed in Supplementary Table 1. The protein levels of IL-6 (Abcam) and TNF-α (Abcam) were measured in the liver according to the manufacturer's recommendations.

Muscle cross-sectional area. Fixed samples of tibialis anterior and soleus muscles were cryosectioned (10 µm-thick cryosections taken at the mid-belly of the muscles) and processed for immunostaining, as described previously⁵. Briefly, sections were blocked for 1 h at room temperature and incubated overnight at 4 °C with a rabbit anti-laminin antibody (Sigma, L9393), followed by incubation with a secondary antibody (AlexFluor Goat anti Rabbit IgG Alexa Fluor 594 -A11012 ThermoFisher). The 10× magnification images were taken using a BX63 Olympus upright microscope. The Fiji software was configured to take into account only the transverse fibers with a Ferret ratio strictly up to 0.5. The muscle fiber area was measured in µm².

Oil Red O stain was used to determine the presence of lipid accumulation in the muscle tissue. Cryosections were rinsed in 60% isopropanol before staining with Oil Red O stain solution. Stain solution is prepared from a stock solution (0.5 g Oil Red O in 100 ml isopropanol) dissolved 3:2 in dH₂O. Slides were incubated for 15 min in stain solution, before rinsing with 60% isopropanol.

The muscle typology was determined by the staining of the ATPase myosin. Briefly, 10 µm frozen muscle sections were pre-incubated in a calcium chloride solution (pH 4.2) for 4 min, washed twice for 30 s with Tris buffer (pH 7.8) and incubated for 25 min at 37 °C in a calcium chloride solution (pH 9.4) containing glycine buffer and 2.75 mM ATP disodium salt (Sigma-Aldrich, A2383). The sections were immersed 4 times for 30 s in a calcium chloride solution and incubated in a cobalt chloride solution for 3 min. Ammonium sulphide at 1% (v/v) (Santa Cruz Biotechnology, sc-214536) was used to precipitate cobalt into a new incubation bath. The frozen sections were then rinsed with water for 5 min and incubated in deionized water. The sections were soaked

in 70/90/100% ethanol and mounted with Canadian balm mounting medium. At the end of the procedure, the Type I fibers were dark brown while the Type II fibers were colorless. Both types were counted manually and a percentage was calculated on each muscle area.

Bone microarchitecture and cortical porosity. Microarchitecture was assessed for the cortical and trabecular bone of the femur (diaphysis and distal metaphysis, respectively), using high-resolution micro-Computed Tomography (VivaCT40, Scanco Medical) at $10.5\ \mu\text{m}^3$ isotropic cubic resolution⁵⁴. Data were acquired at 70 keV, with a 114 mA current and integration time of 275 ms. Three-dimensional reconstructions were generated using the following parameters: $\sigma = 1.2$; support = 2; threshold = 120 for trabecular bone and 0.8, 1, 260 for cortical bone.

The following structural parameters of cortical (Ct.) bone were measured from a stack of 60 sections: cortical porosity ($\text{Ct.porosity} = (1 - (\text{bone volume} / \text{total volume} (\text{BV}/\text{TV}), \%)$), cortical thickness (Ct.Th, mm), cortical tissue mineral density (TMD, mg of hydroxyapatite (HA)/ cm^3). The following parameters of trabecular (Tb.) bone were measured from a stack of 150 sections: trabecular spacing (Tb.Sp), trabecular number (Tb.N., mm^{-1}) and trabecular thickness (Tb.Th, mm), trabecular bone volume / total volume (Tb.BV/TV, %).

Statistical analysis. GraphPad Prism 8 (GraphPad Inc.) was used to analyze the data. All quantitative data are expressed as the mean \pm standard error of mean (SEM). Distributions were tested for normality using the D'Agostino-Pearson test. All individual points are shown. All variables were analyzed using one-way ANOVA as the independent variables. P value < 0.05 was considered to indicate statistically significant differences.

Data availability

The dataset is available on reasonable request from the corresponding author.

Received: 26 August 2022; Accepted: 20 March 2023

Published online: 04 April 2023

References

- Stenvinkel, P., Carrero, J. J., von Walden, F., Ikizler, T. A. & Nader, G. A. Muscle wasting in end-stage renal disease promulgates premature death: established, emerging and potential novel treatment strategies. *Nephrol Dial Transpl.* **31**(7), 1070–1077. <https://doi.org/10.1093/ndt/gfv122> (2016).
- Beddhu, S., Pappas, L. M., Ramkumar, N. & Samore, M. Effects of body size and body composition on survival in hemodialysis patients. *J Am Soc Nephrol JASN.* **14**(9), 2366–2372 (2003).
- Wilhelm-Leen ER, Hall YN, K Tamura M, Chertow GM. Frailty and chronic kidney disease: the Third National Health and Nutrition Evaluation Survey. *Am J Med.* 2009;122(7):664–671. doi:<https://doi.org/10.1016/j.amjmed.2009.01.026>
- Wang, X. H. & Mitch, W. E. Mechanisms of muscle wasting in chronic kidney disease. *Nat Rev Nephrol.* **10**(9), 504–516. <https://doi.org/10.1038/nrneph.2014.112> (2014).
- Benoit, B. *et al.* Fibroblast growth factor 19 regulates skeletal muscle mass and ameliorates muscle wasting in mice. *Nat Med.* **23**(8), 990–996. <https://doi.org/10.1038/nm.4363> (2017).
- Pereira S da C, Benoit B, de Aguiar Junior FCA, *et al.* Fibroblast growth factor 19 as a countermeasure to muscle and locomotion dysfunctions in experimental cerebral palsy. *J Cachexia Sarcopenia Muscle.* Published online October 26, 2021. doi:<https://doi.org/10.1002/jcsm.12819>
- Bozadjieva-Kramer, N. *et al.* Intestinal-derived FGF15 protects against deleterious effects of vertical sleeve gastrectomy in mice. *Nat Commun.* **12**(1), 4768. <https://doi.org/10.1038/s41467-021-24914-y> (2021).
- Degriolamo, C., Sabbà, C. & Moschetta, A. Therapeutic potential of the endocrine fibroblast growth factors FGF19, FGF21 and FGF23. *Nat Rev Drug Discov.* **15**(1), 51–69. <https://doi.org/10.1038/nrd.2015.9> (2016).
- Kir, S. *et al.* FGF19 as a postprandial, insulin-independent activator of hepatic protein and glycogen synthesis. *Science* **331**(6024), 1621–1624. <https://doi.org/10.1126/science.1198363> (2011).
- Inagaki, T. *et al.* Fibroblast growth factor 15 functions as an enterohepatic signal to regulate bile acid homeostasis. *Cell Metab.* **2**(4), 217–225. <https://doi.org/10.1016/j.cmet.2005.09.001> (2005).
- Lan, T. *et al.* FGF19, FGF21, and an FGFR1/ β -klotho-activating antibody act on the nervous system to regulate body weight and glycemia. *Cell Metab.* **26**(5), 709–718.e3. <https://doi.org/10.1016/j.cmet.2017.09.005> (2017).
- Guo, A. *et al.* FGF19 protects skeletal muscle against obesity-induced muscle atrophy, metabolic derangement and abnormal iris levels via the AMPK/SIRT-1/PGC- α pathway. *J Cell Mol Med.* **25**(7), 3585–3600. <https://doi.org/10.1111/jcmm.16448> (2021).
- Fu, L. *et al.* Fibroblast growth factor 19 increases metabolic rate and reverses dietary and leptin-deficient diabetes. *Endocrinology* **145**(6), 2594–2603. <https://doi.org/10.1210/en.2003-1671> (2004).
- Guthrie G, Vonderohe C, Burrin D. Fibroblast growth factor 15/19 expression, regulation, and function: an overview. *Mol Cell Endocrinol.* 2022;548:111617. doi:<https://doi.org/10.1016/j.mce.2022.111617>
- Marchelek-Myśliwiec, M. *et al.* Chronic kidney disease is associated with increased plasma levels of fibroblast growth factors 19 and 21. *Kidney Blood Press Res.* **44**(5), 1207–1218. <https://doi.org/10.1159/000502647> (2019).
- Li M, Qureshi AR, Ellis E, Axelsson J. Impaired postprandial fibroblast growth factor (FGF)-19 response in patients with stage 5 chronic kidney diseases is ameliorated following antioxidative therapy. *Nephrol Dial Transplant.* 2013;28(suppl_4):iv212–iv219. doi:<https://doi.org/10.1093/ndt/gft337>
- Reiche, M. *et al.* Fibroblast growth factor 19 serum levels: relation to renal function and metabolic parameters. *Horm Metab Res Horm Stoffwechselforschung Horm Metab.* **42**(3), 178–181. <https://doi.org/10.1055/s-0029-1243249> (2010).
- Koppe, L. *et al.* Urea impairs β cell glycolysis and insulin secretion in chronic kidney disease. *J Clin Invest.* **126**(9), 3598–3612. <https://doi.org/10.1172/JCI86181> (2016).
- Cheung, W. W. *et al.* A pegylated leptin antagonist ameliorates CKD-associated cachexia in mice. *J Am Soc Nephrol.* **25**(1), 119–128. <https://doi.org/10.1681/ASN.2013040432> (2014).
- Heveran, C. M. *et al.* Chronic kidney disease and aging differentially diminish bone material and microarchitecture in C57Bl/6 mice. *Bone* **127**, 91–103. <https://doi.org/10.1016/j.bone.2019.04.019> (2019).
- Palacios-Ramirez R, Lima-Posada I, Bonnard B, *et al.* Mineralocorticoid receptor antagonism prevents the synergistic effect of metabolic challenge and chronic kidney disease on renal fibrosis and inflammation in mice. *Front Physiol.* 2022;13:859812. doi:<https://doi.org/10.3389/fphys.2022.859812>

22. Xie, Y. *et al.* Higher blood urea nitrogen is associated with increased risk of incident diabetes mellitus. *Kidney Int.* **93**(3), 741–752. <https://doi.org/10.1016/j.kint.2017.08.033> (2018).
23. Bailey, J. L., Zheng, B., Hu, Z., Price, S. R. & Mitch, W. E. Chronic kidney disease causes defects in signaling through the insulin receptor substrate/phosphatidylinositol 3-kinase/Akt pathway: implications for muscle atrophy. *J Am Soc Nephrol JASN.* **17**(5), 1388–1394. <https://doi.org/10.1681/ASN.2004100842> (2006).
24. Pedersen, B. K. & Febbraio, M. A. Muscles, exercise and obesity: skeletal muscle as a secretory organ. *Nat Rev Endocrinol.* **8**(8), 457–465. <https://doi.org/10.1038/nrendo.2012.49> (2012).
25. Yanishi, M. *et al.* Factors related to osteosarcopenia in kidney transplant recipients. *Transpl. Proc.* **50**(10), 3371–3375. <https://doi.org/10.1016/j.transproceed.2018.04.032> (2018).
26. Binkley, N. & Buehring, B. Beyond FRAX: it's time to consider "sarco-osteopenia". *J Clin Densitom Off J Int Soc Clin Densitom.* **12**(4), 413–416. <https://doi.org/10.1016/j.jocd.2009.06.004> (2009).
27. Koppe, L. *et al.* p-Cresyl sulfate promotes insulin resistance associated with CKD. *J Am Soc Nephrol JASN.* **24**(1), 88–99. <https://doi.org/10.1681/ASN.2012050503> (2013).
28. Chowdhury, S. *et al.* Muscle-derived interleukin 6 increases exercise capacity by signaling in osteoblasts. *J Clin Invest.* **130**(6), 2888–2902. <https://doi.org/10.1172/JCI133572> (2020).
29. Zhang, L. *et al.* Stat3 activation links a C/EBP δ to myostatin pathway to stimulate loss of muscle mass. *Cell Metab.* **18**(3), 368–379. <https://doi.org/10.1016/j.cmet.2013.07.012> (2013).
30. Bailey, J. L. *et al.* The acidosis of chronic renal failure activates muscle proteolysis in rats by augmenting transcription of genes encoding proteins of the ATP-dependent ubiquitin-proteasome pathway. *J. Clin. Invest.* **97**(6), 1447–1453. <https://doi.org/10.1172/JCI118566> (1996).
31. Tamaki, M. *et al.* Chronic kidney disease reduces muscle mitochondria and exercise endurance and its exacerbation by dietary protein through inactivation of pyruvate dehydrogenase. *Kidney Int.* **85**(6), 1330–1339. <https://doi.org/10.1038/ki.2013.473> (2014).
32. Lewis, M. I. *et al.* Metabolic and morphometric profile of muscle fibers in chronic hemodialysis patients. *J Appl Physiol.* **112**(1), 72–78. <https://doi.org/10.1152/jappphysiol.00556.2011> (2012).
33. Zhang, L. *et al.* Pharmacological inhibition of myostatin suppresses systemic inflammation and muscle atrophy in mice with chronic kidney disease. *FASEB J.* **25**(5), 1653–1663. <https://doi.org/10.1096/fj.10-176917> (2011).
34. Rubinfeld, S. & Garber, A. J. Abnormal carbohydrate metabolism in chronic renal failure: the potential role of accelerated glucose production, increased gluconeogenesis, and impaired glucose disposal. *J Clin Invest.* **62**(1), 20–28. <https://doi.org/10.1172/JCI109107> (1978).
35. Chapagain, A. *et al.* Elevated hepatic 11 β -hydroxysteroid dehydrogenase type 1 induces insulin resistance in uremia. *Proc Natl Acad Sci USA* **111**(10), 3817–3822. <https://doi.org/10.1073/pnas.1312436111> (2014).
36. Harrison, S. A. *et al.* NGM282 for treatment of non-alcoholic steatohepatitis: a multicentre, randomised, double-blind, placebo-controlled, phase 2 trial. *Lancet Lond Engl.* **391**(10126), 1174–1185. [https://doi.org/10.1016/S0140-6736\(18\)30474-4](https://doi.org/10.1016/S0140-6736(18)30474-4) (2018).
37. Luce, M. *et al.* Accumulation of natriuretic peptides is associated with protein energy wasting and activation of brown fat in white adipose tissue in chronic kidney disease. *Kidney Int.* **98**(3), 663–672. <https://doi.org/10.1016/j.kint.2020.03.027> (2020).
38. Zhou, M. *et al.* Engineered fibroblast growth factor 19 reduces liver injury and resolves sclerosing cholangitis in Mdr2-deficient mice. *Hepatology* **63**(3), 914–929. <https://doi.org/10.1002/hep.28257> (2016).
39. Schaefer, F., Chen, Y., Tsao, T., Nouri, P. & Rabkin, R. Impaired JAK-STAT signal transduction contributes to growth hormone resistance in chronic uremia. *J Clin Invest.* **108**(3), 467–475. <https://doi.org/10.1172/JCI11895> (2001).
40. Kopple, J. D. *et al.* OPPORTUNITY™: a large-scale randomized clinical trial of growth hormone in hemodialysis patients. *Nephrol Dial Transpl. Off Publ Eur Dial Transpl Assoc - Eur Ren Assoc.* **26**(12), 4095–4103. <https://doi.org/10.1093/ndt/gfr363> (2011).
41. Asai, O. *et al.* Decreased renal α -Klotho expression in early diabetic nephropathy in humans and mice and its possible role in urinary calcium excretion. *Kidney Int.* **81**(6), 539–547. <https://doi.org/10.1038/ki.2011.423> (2012).
42. Yamamoto, S. *et al.* Serum endocrine fibroblast growth factors as potential biomarkers for chronic kidney disease and various metabolic dysfunctions in aged patients. *Intern Med Tokyo Jpn.* **59**(3), 345–355. <https://doi.org/10.2169/internalmedicine.3597-19> (2020).
43. Sun, L., Cai, J. & Gonzalez, F. J. The role of farnesoid X receptor in metabolic diseases, and gastrointestinal and liver cancer. *Nat Rev Gastroenterol Hepatol.* **18**(5), 335–347. <https://doi.org/10.1038/s41575-020-00404-2> (2021).
44. Koppe, L., Mafra, D. & Fouque, D. Probiotics and chronic kidney disease. *Kidney Int.* **88**(5), 958–966. <https://doi.org/10.1038/ki.2015.255> (2015).
45. Gai, Z. *et al.* Effect of chronic renal failure on the hepatic, intestinal, and renal expression of bile acid transporters. *Am J Physiol Renal Physiol.* **306**(1), F130–137. <https://doi.org/10.1152/ajprenal.00114.2013> (2014).
46. Uchiyama, K. *et al.* Contribution of uremic dysbiosis to insulin resistance and sarcopenia. *Nephrol Dial Transpl. Off Publ Eur Dial Transpl Assoc - Eur Ren Assoc.* **35**(9), 1501–1517. <https://doi.org/10.1093/ndt/gfaa076> (2020).
47. Thome T, Kumar RA, Burke SK, *et al.* Impaired muscle mitochondrial energetics is associated with uremic metabolite accumulation in chronic kidney disease. *JCI Insight.* 2020;6(1). doi:<https://doi.org/10.1172/jci.insight.139826>
48. Jia, W. H. *et al.* Effect of skeletal muscle phenotype and gender on fasting-induced myokine expression in mice. *Biochem Biophys Res Commun.* **514**(2), 407–414. <https://doi.org/10.1016/j.bbrc.2019.04.155> (2019).
49. Berru, F. N. *et al.* Chronic kidney disease exacerbates ischemic limb myopathy in mice via altered mitochondrial energetics. *Sci Rep.* **9**(1), 15547. <https://doi.org/10.1038/s41598-019-52107-7> (2019).
50. Chen, J. *et al.* Fibroblast growth factor 19-mediated up-regulation of SYR-related high-mobility group box 18 promotes hepatocellular carcinoma metastasis by transactivating fibroblast growth factor receptor 4 and Fms-related tyrosine kinase 4. *Hepatology* **71**(5), 1712–1731. <https://doi.org/10.1002/hep.30951> (2020).
51. Kuro-O, M. The Klotho proteins in health and disease. *Nat Rev Nephrol.* **15**(1), 27–44. <https://doi.org/10.1038/s41581-018-0078-3> (2019).
52. Niu, J. *et al.* Curtailing FGF19's mitogenicity by suppressing its receptor dimerization ability. *Proc Natl Acad Sci USA.* **117**(46), 29025–29034. <https://doi.org/10.1073/pnas.2010984117> (2020).
53. Barba, C. *et al.* A low aromatic amino-acid diet improves renal function and prevent kidney fibrosis in mice with chronic kidney disease. *Sci Rep.* **11**(1), 19184. <https://doi.org/10.1038/s41598-021-98718-x> (2021).
54. Bouleftour, W. *et al.* Deletion of OPN in BSP knockout mice does not correct bone hypomineralization but results in high bone turnover. *Bone* **120**, 411–422. <https://doi.org/10.1016/j.bone.2018.12.001> (2019).

Acknowledgements

We acknowledge the training and technical support of Norbert Laroche with microCT analysis.

Author contributions

B.B., A.B., E.B. and L.K. carried out the experiment and contributed to the interpretation of the results. B.B., H.V., J.R., L.V. and L.K. conceived the original idea and were in charge of overall direction and planning. C.P.

help for animals monitoring. M.S., P.G., H.Z. provided the bone analysis. S.C. and A.V.M. performed histological analysis. A.J. performed biochemical assay and RNA analyses. L.K., B.B. and H.V. supervised the findings of this work and the manuscript writing. All authors reviewed and approved the final version. L.K. is the guarantor of this work and accept full responsibility for the conduct of the study.

Funding

This work was supported by the French National Research Agency (ANR-19-CE14-0017-01, Project BONTON-19), the Société Francophone de Néphrologie Dialyse Transplantation (SFNDT) and Institut National de la Santé et de la Recherche Médicale (INSERM). EB was supported by a grant from the “Année recherche, Hospices Civils de Lyon”. LV and MS were also supported by ARMOE (Aide à la Recherche Médicale Ondaine et Environs) (2018) and MS by Fonds d’amorçage Recherche de la Fondation UJM.

Competing interests

The authors declare no competing interests.

Additional information

Supplementary Information The online version contains supplementary material available at <https://doi.org/10.1038/s41598-023-31874-4>.

Correspondence and requests for materials should be addressed to L.K.

Reprints and permissions information is available at www.nature.com/reprints.

Publisher’s note Springer Nature remains neutral with regard to jurisdictional claims in published maps and institutional affiliations.



Open Access This article is licensed under a Creative Commons Attribution 4.0 International License, which permits use, sharing, adaptation, distribution and reproduction in any medium or format, as long as you give appropriate credit to the original author(s) and the source, provide a link to the Creative Commons licence, and indicate if changes were made. The images or other third party material in this article are included in the article’s Creative Commons licence, unless indicated otherwise in a credit line to the material. If material is not included in the article’s Creative Commons licence and your intended use is not permitted by statutory regulation or exceeds the permitted use, you will need to obtain permission directly from the copyright holder. To view a copy of this licence, visit <http://creativecommons.org/licenses/by/4.0/>.

© The Author(s) 2023